

The Use of Small Telescopes for Spectral Imaging of Low-light-level Extended Atmospheres in the Solar System

Jeffrey Baumgardner · Michael Mendillo

Received: 23 January 2009 / Accepted: 2 May 2009 / Published online: 7 July 2009
© Springer Science+Business Media B.V. 2009

Abstract A 10-cm aperture telescope equipped with coronagraphic capabilities, using occulting masks of various size and material, has been developed to obtain low-light-level, wide-angle ($\sim 7^\circ$ FOV), narrow-band filtered images of sodium exospheres at Io, the Moon and Mercury. Here we describe new instrument capabilities and recent findings about the extraordinarily long tails of sodium gas discovered in the lunar and hermean exospheres. Spatial and temporal variability patterns captured in such images can be used to study changes in surface sputtering processes and radiation pressure acceleration effects in the inner solar system.

Keywords Planetary exospheres · Sodium · Coronagraphic imaging

1 Introduction

Telescopic astronomy began with Galileo's observations in 1609, creating a revolution in how we view Nature. As the principles of optics and telescope design advanced, emphasis was directed entirely towards light-gathering power and angular resolution. No options were available for improvement upon the detector system, i.e., the human eye that recorded data at the end of the optical axis until photography emerged in the nineteenth century. By that time, the apertures of state-of-the-art telescopes were approximately 0.5 m. The era of the 50-m class telescope is now in active development. While a 100-fold increase in telescope aperture is a most impressive accomplishment in ~ 150 years, the technology of detectors, from Daguerreotype to the best modern charge-coupled-device (CCD), has resulted in ~ 1 million-fold increase in the ability (sensitivity) to record light over, approximately, the same time span.

Given that the technology of bigger and better telescopes advanced sooner than that of detector design, the possible evolutionary step of using the best possible CCD on a small telescope was slow to be embraced by professional astronomers. In our initial treatment of

J. Baumgardner (✉) · M. Mendillo
Center for Space Physics, Boston University, Boston, MA 02215, USA
e-mail: jeffreyb@bu.edu

this topic (Baumgardner and Mendillo 1993), we speculated on what Galileo might have published in *Siderius Nuncius* (1610) if he had used a CCD in place of his eye and great drawing skills. Within a generation of Galileo's death, apertures of 0.1 m were common. Even a century later, Carolyn Herschel used a 0.1 m Newtonian reflector telescope, with a field of view of $\sim 2^\circ$, to discover visually the great comet of 1786, and within a decade seven more (Holmes 2008). What might she have found with this fine instrument equipped with a CCD camera?

Here we report on the use of an eighteenth century Herschellian class telescope (0.1 m refractor) equipped with a twenty-first century CCD detector system, further augmented by the use of modern interference filters and image processing methods. Such an instrument has a particular niche to fill when directed towards low-light-level, wide field-of-view (FOV) targets within the solar system. As with Ms. Herschel, such a telescope is not well suited for studying the surfaces of planets or moons, but remarkably so for the comet-like comas and tails they might have.

2 Instrument

Figure 1 gives a schematic depiction of the telescope system developed to enable studies of extended gaseous structures in the solar system. The key challenge to the design was to optimize simultaneously light-gathering-power (large aperture), wide-angle coverage (short focal length), and the use of narrow band filters (requiring small departures from perpendicularity of rays striking the filter). In addition, occulting masks of various sizes are needed to block light from Jupiter and its Galilean moons (6-arc min in size), and from our Moon (~ 30 -arc min in size).

The telescope is composed of two parts: a unity power section that serves as the coronagraph; and a fast F/1.2, 85 mm F.L. lens coupled to a CCD that is the telescope/detector.

The front element of the coronagraph section is a cemented achromat chosen to minimize the scattered light from its two exterior surfaces. The very bright image of the primary body (e.g. the Moon or Mercury) falls on the occulting mask so photons from the bright image are prevented from scattering from the multitude of surfaces farther down the optical path. The light rays passing through this first image plane are then collimated by a second achromat identical to the front element. The light from the edge of the field of view

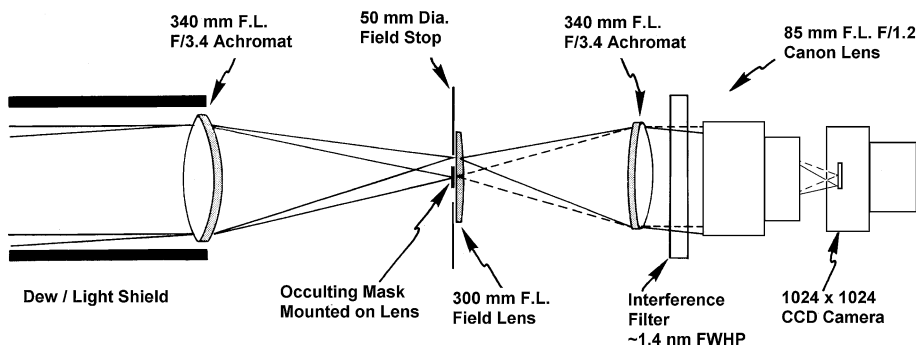


Fig. 1 Schematic of the Boston University coronagraphic filtered imaging system developed for studies of solar system exospheres

is directed towards the collimator by a field lens at the first focal plane that also serves as a mounting surface for the occulting mask. The field of view is limited by a 50 mm diameter stop such that no light ray passes through the interference filter at an angle greater than $\sim 4^\circ$. Since the band-pass of interference filters shift to shorter wavelengths with increasing angles of incidence, this 4° angle allows the band pass to be ~ 1.4 nm without excluding the wavelengths of interest. These 100 mm diameter filters are mounted in a filter wheel that allows for the selection of 4 different wavelengths, e.g., on-band and off-band, so that just the signal from the spectral line of interest can be derived.

This instrument was, at first, fitted with an intensified CCD. The current detector has a thinned, back side illuminated, $1024 \times 1024 \times 13$ micron pixel CCD housed in a Peltier cooled housing. The dark signal is ~ 0.05 electrons/s at -25°C , and the read noise is ~ 9 electrons (rms). For the images shown in this article the detector was binned 2×2 to increase sensitivity. A typical exposure time would be 10 s to several minutes depending on the brightness of the signal near the mask.

The observing site at the McDonald Observatory (30.671 N, 104.023 W) is at an elevation of 2,000 m. A typical observing run of ~ 5 days would experience at least 1 day of excellent transparency, a necessary condition for coronagraphic observations. The relative humidity usually is below 10% for these observations and no smoke, haze, or thin cirrus can be present for quality data to be taken.

The reduction of the data from a typical set of observations involves the usual steps of bias/dark corrections as well as the subtraction of an off-band image from the data image to remove the large scattered light component (tropospheric as well as instrumental) from the on-band image. For the sodium data reported here, the off-band filter is centered at 605 nm. Since the instrument has a slightly different responsivity at the off-band wavelength due to differences in Q.E. of the detector and different filter characteristics, and the fact that the scattered light at the sodium wavelength has the strong D1 and D2 absorption lines present, the off-band image must be scaled before subtraction. A short exposure of the disk of the Moon or a solar type star is used to determine this factor.

The reduction of the data to Rayleighs is accomplished by using standard stars whose fluxes at the given wavelengths are known. An alternate method used in the past relied on a standard lamp (C^{14} activated phosphor) to determine the responsivity of the instrument. (see Mendillo et al. 2004, for additional details on data reduction techniques.)

3 Application to the Moon's Exosphere

Using spectroscopic techniques, the Moon was found to have a tenuous atmosphere of sodium gas (Potter and Morgan 1988). With a particle density of $50\text{--}100/\text{cm}^3$ at the surface, out of an estimated total gas population of $\sim 10^5/\text{cm}^3$, sodium is a minor constituent of the remarkably thin lunar atmosphere. Yet, it is useful as a tracer by virtue of its strong resonantly scattering cross-section for sunlight at 589 nm and 589 nm (Chamberlain and Hunten 1987). The Na atoms are sputtered off the surface continuously by the impact of sunlight, micro-meteors and solar wind plasma. Ejection speeds can be comparable to the Moon's low escape speed (2.3 km/s), and thus their trajectories can reach high altitudes prior to subsequent re-impact of the regolith. While aloft, some of the atoms are photo-ionized and carried away by the solar wind, while others experience strong solar radiation pressure acceleration to form a tail of escaping neutral gas. The lunar atmosphere is thus called a surface-boundary-exosphere (SBE) (Stern 1999).

To image the full 2-dimensional pattern of the Moon's sodium exosphere presents an observational problem analogous to photographing the Sun's corona, i.e., a large faint region surrounding an extremely bright object. The coronagraphic imager shown in Fig. 1, with its lunar size occulting mask, was used to map the lunar corona out to $\sim 5 R_{\text{moon}}$ (Flynn and Mendillo 1993). During lunar eclipses (when the bright source of scattered light is minimal), the exosphere was mapped out to $10\text{--}20 R_{\text{moon}}$, i.e., spanning 10° of sky (Mendillo and Baumgardner 1995; Wilson et al. 2006).

With multi-national initiatives underway for a return to a human presence on the Moon, lunar exosphere science now focuses on the near-disk sodium, as well as its escaping tail. The former requires much improved ways to specify Na versus altitude above the limb. The opaque occulting mask used previously was adequate for approximating the Moon's position behind the mask via the use of star locations captured in the image. For more precise registration of the Moon's exact location during an observation, the instrument now has a mask made of gelatin neutral density filter material (Wratten #96 optical density 2.0). Results of our initial test of this new approach are shown in Fig. 2. Clearly, the surface of the Moon can now be imaged at the same time as its atmosphere, thereby allowing little ambiguity in their spatial relationship.

The image in Fig. 2 clearly shows that solar radiation pressure distorts a classic coma of escaping gas, with Na visible above and below the Moon's physical shadow region. These atoms lead to a tail that can be observed directly on days near 1st and 3rd quarter Moon. At these times, however, the tail is observed essentially perpendicular to its anti-sunward axis, and thus the low cross-tail column contents of Na have brightness levels too low to record at distances beyond several lunar radii. At the time of new Moon, however, the lunar tail is directed anti-sunward towards the Earth. As this ensemble of Na atoms encounters terrestrial gravity, the streaming particles are partially focused into a beam or enhanced column of gas beyond Earth that is aligned along the Sun–Moon–Earth axis. When viewed from the night side of the Earth, a *lunar sodium spot* of $2\text{--}3^\circ$ in size is visible as the tail-

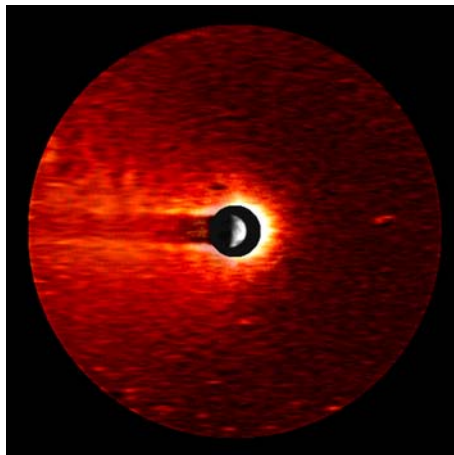


Fig. 2 Initial result from the use of the telescope in Fig. 1 equipped with a neutral density filter for its occulting mask and sodium filter to observe the lunar exosphere. The dark band to the left is the Moon's shadow cast onto the sodium atoms streaming away from the Moon under the influence of solar radiation pressure (see text). This image is the result of the registration and co-addition of 15 one-minute exposures. This new system allows for both the exact position of the lunar limb and the distribution of sodium gas (coma and tail lobes) to be recorded in the same image

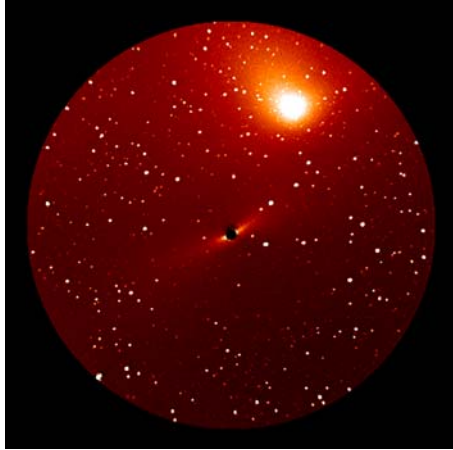


Fig. 3 Image taken at 6 UT on the night of 8 April 2005 when the sodium nebula of the Jupiter-Io system was visible within the same $\sim 7^\circ$ FOV as the Moon's extended sodium tail spot. Jupiter was near opposition and the Moon was near new phase as the gravitationally focused beam of lunar sodium atoms swept through the field of view during the night. Jupiter and its moons are behind an opaque occulting mask at the center of the FOV. The center of the moon-spot is along the Sun-Earth-Moon line (see text). This image is the sum of 20 two-minute exposures

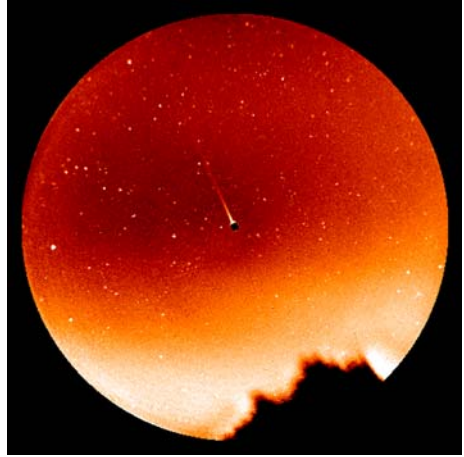
column-integrated signature of the Moon's escaping exosphere (Smith et al. 1999; Wilson et al. 1999; Mierkiewicz et al. 2006; Matta et al. 2009).

Figure 3 offers a rare view of two solar system exospheres within the same 7° FOV. On April 8, 2005, Jupiter was almost exactly in opposition when the Moon was in new phase. Thus, Jupiter's great sodium magneto-nebula (Mendillo et al. 1990, 2004) and the Moon's sodium tail spot were both visible in the anti-sunward direction. These large-scale features, produced in drastically different ways (via Io's volcanism versus micro-meteor sputtering of the lunar regolith), have brightness values of comparable values (50–100 Rayleighs(R), where $1R = 10^6$ photons/s/cm²/4 π steradians, (Chamberlain and Hunten 1987). Long term observations of both exospheres to document temporal variability in source rates are currently underway using this telescope.

4 Exospheric Science at Mercury

The Moon and Mercury share many characteristics, among them ancient regoliths subjected to sputtering processes that produce surface boundary exospheres (Hunten and Sprague 1997; Killen and Ip 1999; Kameda et al. 2008; Ip and Wang 2008). Leblanc et al. (2007) have summarized processes acting at Mercury, with particular attention to those mapped by sodium emissions. As with the Moon, a tail of Na atoms was discovered by Potter et al. (2002) that extended to their limits of detection at about 16 R_{Mer} . Using the instrument in Fig. 1, the tail has now been mapped out to $\sim 1,500 R_{Mer}$ (Baumgardner et al. 2008). A major difference between Mercury and the Earth–Moon system is that the latter have nearly circular orbits and thus lunar Na atoms do not experience pronounced changes, via radial velocity effects, in solar radiation acceleration. Mercury's orbit is far more elliptical and thus the periodicity in radial velocity between it and the Sun results in Na atoms experiencing strong/weak radiation pressure conditions via Doppler shifting out

Fig. 4 Sodium image taken of Mercury at low elevation angle (trees show horizon) at dusk on 31 May 2007, with the planet behind the 6' occulting mask used for Jupiter/Io observations. The image is the result of three, two-minute exposures. A tail of $\sim 2^\circ$ is visible in the anti-sunward direction. The occulting mask hides $\sim 35 R_{\text{Mer}}$, with the tail visible beyond $1400 R_{\text{Mer}}$ or 3.4×10^6 km (from Baumgardner et al. 2008)



of/into the solar Fraunhofer absorption lines at 589.0 and 589.6 nm. Thus, Mercury's sodium tail can be remarkably long or dramatically short, depending upon its orbital position (Smyth and Marconi 1995; Potter et al. 2007). Under conditions most favorable for tail extent, ~ 5 – 10 days after perihelion passage (as in Fig. 4), the variation in brightness down the tail axis might be related to the time history of source changes on the planet (Baumgardner et al. 2008). During the first fly-by of Mercury by the MESSENGER spacecraft (7 January 2008), a time of minimal solar radiation pressure, a tail of modest length ($\sim 10 R_{\text{Mer}}$) was detected by the MASCS UVVS instrument (McClintock et al. 2008). Ground-based observations using the system in Fig. 1 found no evidence of the tail beyond the edge of the occulting mask, a distance of $\sim 135 R_{\text{Mer}}$ at that time; yet additional cases of extremely long tails were found in orbital positions comparable to that in Fig. 4 (Schmidt et al. 2009). In preparations for the BepiColombo mission to Mercury, a systematic set of sodium observations are underway by the International Mercury Watch (IMW) team (Mendillo et al. 2007; Okano et al. 2008).

This 10 cm coronagraph system also has been used to image faint emissions at wavelengths other than 589.0 and 589.6 nm. H-alpha (656.3 nm) images have been made (Baumgardner and Mendillo 1993) of galactic HII regions as well as H_2O^+ (619.9 nm) images of comet Hale-Bopp (Wilson et al. 1998). Currently, an effort is under way to search for hydrogen emissions surrounding Saturn.

Acknowledgements This work was supported, in part, by the NASA Planetary Astronomy program and by seed research funds through the Center for Space Physics at Boston University. We thank Jody Wilson, Majd Matta and Carl Schmidt for their assistance in several aspects of this work.

References

- J. Baumgardner, J. Wilson, M. Mendillo, Imaging the sources and full extent of the sodium tail of the planet Mercury. *Geophys. Res. Lett.* **35** (2008). doi:10.1029/2007GL032337
- J. Baumgardner, M. Mendillo, If Galileo had owned a CCD. *Sky Telesc.* **85**(6), 19–21 (1993)
- J.W. Chamberlain, D.M. Hunten, *Theory of Planetary Atmospheres*, 2nd edn. (Academic Press, Inc., Orlando, FL, 1987)
- B. Flynn, M. Mendillo, A picture of the Moon's atmosphere. *Science* **261**, 184–186 (1993)
- R. Holmes, *The Age of Wonder* (Harper Press, London, 2008)

- D.M. Hunten, A.L. Sprague, Origin and character of the lunar and mercurian atmospheres. *Adv. Space Res.* **19**(10), 1551–1560 (1997)
- W.-H. Ip, Y.-C. Wang, A comparison of the exospheres of Mercury and the Moon. *Adv. Space Res.* **42**, 34–39 (2008)
- S. Kameda, Kagitani, M., Okano S., Yoshikawa, I., Ono, J.: Observations of Mercury's sodium tail using a Fabry-Perot interferometer. *Adv. Space Res.* **41**, 1381–1385 (2008)
- R.M. Killen, W.H. Ip, The surface-bounded atmospheres of Mercury and the The Moon. *Rev. Geophys.* **37**, 361–406 (1999)
- F. Leblanc et al., Mercury's exosphere origins and relations to its magnetosphere and surface. *Planet. Space Sci.* **55**, 1069–1092 (2007). doi:[10.1016/j.pass.2006.11.008](https://doi.org/10.1016/j.pass.2006.11.008)
- M. Matta, S. Smith, J. Wilson, J. Baumgardner, M. Mendillo, The sodium tail of the Moon. *Icarus* (2009) (in press)
- M. Mendillo, J. Baumgardner, Constraints on the origin of the Moon's atmosphere from observations during a lunar eclipse. *Nature* **377**, 404–406 (1995)
- M. Mendillo, International Mercury Watch (IMW) team, Preliminary results of the 2006 campaign, European Geoscience Union (EGU) meeting, Vienna. *Geophys. Res. Abstr.* **9**, 05797 (2007)
- M. Mendillo, J. Baumgardner, B. Flynn, J. Hughes, The extended sodium nebula of Jupiter. *Nature* **348**, 312–314 (1990)
- M. Mendillo, J. Wilson, S. Spencer, J. Stansberry, Io's volcanic control of Jupiter's extended neutral clouds. *Icarus* **170**, 4430–4442 (2004)
- W.E. McClintock et al., Mercury's exosphere: Observations during MESSENGER's first Mercury Fly-by. *Science* **321**, 92–94 (2008)
- E.J. Mierkiewicz, M. Line, F.L. Roesler, R.J. Oliverson, Radial velocity observations of the extended lunar sodium tail. *Geophys. Res. Lett.* **33**, L201 (2006). doi:[10.1029/2006GL027650](https://doi.org/10.1029/2006GL027650)
- S. Okano, International Mercury Watch (IMW) team, Preliminary results of the campaign observations of 2007 and 2008, Asia Oceania Geosciences Society (AOGS) meeting, Busan, Korea, 12–16 June 2008
- A.E. Potter, T.H. Morgan, Discovery of sodium and potassium vapor in the atmosphere of the Moon. *Science* **241**, 675–680 (1988)
- A.E. Potter, R.M. Killen, T.H. Morgan, The sodium tail of Mercury. *Meteorit. Planet. Sci.* **37**, 1165–1172 (2002)
- A.E. Potter, R.M. Killen, T.H. Morgan, Solar radiation acceleration effects on Mercury sodium emission. *Icarus* **186**, 571–580 (2007)
- C.J. Schmidt, V. Wilson, J. Baumgardner, M. Mendillo, Mercury's distant sodium tail. *Icarus* (2009) (in press)
- S.M. Smith, J. Wilson, J. Baumgardner, M. Mendillo, Discovery of the distant lunar sodium tail, its enhancement following the Leonid meteor shower of 1998. *Geophys. Res. Lett.* **26**, 1649–1652 (1999)
- W. Smyth, M. Marconi, Theoretical overview and modeling of the sodium and potassium atmospheres of the Moon. *Astrophys. J.* **441**, 839–864 (1995)
- S.A. Stern, The lunar atmosphere: History, status, current problems and context. *Rev. Geophys.* **37**, 453–491 (1999)
- J.K. Wilson, J. Baumgardner, M. Mendillo, Three tails of comet Hale-Bopp. *Geophys. Res. Lett.* **25**, 225–228 (1998)
- J.K. Wilson, S.M. Smith, J. Baumgardner, M. Mendillo, Modeling an enhancement of the lunar sodium atmosphere, tail during the Leonid meteor shower of 1998. *Geophys. Res. Lett.* **26**, 1645–1648 (1999)
- J. Wilson, K.M. Mendillo, H.E. Spence, Magnetospheric influence on the Moon's exosphere. *J. Geophys. Res.* **111**, A07207 (2006). doi:[10.1029/2005JA011364](https://doi.org/10.1029/2005JA011364)